Analysis of Elasto/Visco-Plastic Dynamic Response of General Thin Shells by Means of Overlay Model*

Katsumi TAO** and Shigeo TAKEZONO**

The numerical analysis of the elasto/visco-plastic dynamic response of general thin shells to arbitrary loads is carried out by means of the elasto/visco-plastic overlay model, which is able to express the Bauschinger effect and the strain rate dependence. Namely, Perzyna's equation is used for the constitutive relation of each layer of the overlay model and as a whole, the Bauschinger effect and the influence of viscosity in the plastic range of the material are taken into account. The equations of motion derived from Sanders' nonlinear theory for thin shells by adding the inertia terms are used, and the relationships between strains and displacements where rotations of the shell are considered for the membrane strains are employed. The basic differential equations derived are numerically solved by the finite difference method. As a numerical example, a cylindrical shell under a semisinusoidal external load with respect to time is analyzed, and the results are compared with those in the case of isotropic hardening.

Key Words: Structural Analysis, Inelasticity, Finite Difference Method, Elasto/Visco-Plasticity, Dynamic Response, General Thin Shells, Bauschinger Effect

1. Introduction

In a dynamic response of shell structures subjected to impulsive loads, the influence of viscosity in the plastic range becomes significant owing to high strain rates. Therefore the consideration of the influence of the material viscosity becomes very important in the structural analysis. As for an elasto/visco-plastic dynamic response of shells to time-dependent loads, many investigations have been carried out for not only the axisymmetrical shells[1]~[6] but also for general thin shells[7]. These investigations, however, are mostly based on the assumption that the material shows isotropic work hardening in the plastic range, and the Bauschinger effect of materials is not included in the calculation.

Hence we studied this problem of the shells by the use of the elasto/visco-plastic overlay model. Perzyna's equation[8] is used for the constitutive relation of each layer of the overlay model[9]. We have already analyzed the small deformation elasto/visco-plastic dynamic response of the axisymmetrical shells by the use of this model[10]. In the present paper, the relatively large deformation for the general thin shells to arbitrary loads is treated using this model.

2. Fundamental Equations

Let the undeformed middle surface of a shell be given by the next equations, as shown in Fig. 1,

$$x^i = x^i(\xi_\alpha) \ (i=1, 2, 3 ; \alpha=1, 2), \tag{1}$$

where x^i are Cartesian coordinates in space and ξ_α are curvilinear coordinates on the surface. When ξ_α are orthogonal, the line element ds is given by

$$ds^2 = a_1^2 d\xi_1^2 + a_2^2 d\xi_2^2, \tag{2}$$

where a_1 and a_2 are Lame's parameters.

Adding the inertia terms to the equilibrium equations in Sanders' nonlinear theory for thin shells[11] and eliminating the transverse shear forces Q_1 and Q_2 from these, where the rotatory inertia terms are omitted, we obtain the following equations of motion:

* Received 23rd October, 1989. Paper No. 88-0922A

** Department of Energy Engineering, Toyohashi University of Technology, Tempaku-cho, Toyohashi, 440, Japan

$$\left.\begin{aligned}&(\alpha_2N_{11})_{,1}+(\alpha_1N_{12})_{,2}+\alpha_{1,2}N_{12}-\alpha_{2,1}N_{22}+R_1^{-1}[(\alpha_2M_{11})_{,1}+(\alpha_1M_{12})_{,2}+\alpha_{1,2}M_{12}-\alpha_{2,1}M_{22}]+(\alpha_1/2)[(R_1^{-1}\\&\quad-R_2^{-1})M_{12}]_{,2}-\alpha_1\alpha_2R_1^{-1}(\phi_1N_{11}+\phi_2N_{12})-(\alpha_1/2)[\phi(N_{11}+N_{22})]_{,2}+\alpha_1\alpha_2(P_1-\rho_0h\partial^2U_1/\partial t^2)=0\\&[(1/\alpha_1)\{(\alpha_2M_{11})_{,1}+(\alpha_1M_{12})_{,2}+\alpha_{1,2}M_{12}-\alpha_{2,1}M_{22}\}]_{,1}+[(1/\alpha_2)\{(\alpha_1M_{22})_{,2}+(\alpha_2M_{12})_{,1}+\alpha_{2,1}M_{12}-\alpha_{1,2}M_{11}\}]_{,2}\\&\quad-\alpha_1\alpha_2(R_1^{-1}N_{11}+R_2^{-1}N_{22})-(\alpha_2\phi_1N_{11}+\alpha_2\phi_2N_{12})_{,1}-(\alpha_1\phi_1N_{12}+\alpha_1\phi_2N_{22})_{,2}+\alpha_1\alpha_2(P-\rho_0h\partial^2W/\partial t^2)=0\end{aligned}\right\}\quad(3)$$

Another equation may be obtained by interchanging subscripts 1 and 2 in the first equation. In these equations, the commas mean partial differentiation with respect to ξ_1 or ξ_2, as the subscript following the comma indicates. N_{11}, N_{22}, N_{12} and M_{11}, M_{22}, M_{12} are the resultant stresses and the resultant moments per unit length of the shell, respectively, as shown in Fig. 1. P_1, P_2 and P are the distributed loads per unit area of the shell. R_1 and R_2 are the principal radii of curvature in the direction of ξ_1 and ξ_2 of the middle surface, respectively. The notations h, t and ρ_0 in the inertia terms are thickness of the shell, time and mass density, respectively. ϕ_1, ϕ_2 and ϕ in the nonlinear terms indicate the rotations of the middle surface and are related to U_1, U_2 and W as follows[11]:

$$\phi_1=-\alpha_1^{-1}W_{,1}+R_1^{-1}U_1,\ \phi_2=-\alpha_2^{-1}W_{,2}+R_2^{-1}U_2,\ \phi=1/2(\alpha_1\alpha_2)^{-1}[(\alpha_2U_2)_{,1}-(\alpha_1U_1)_{,2}].\quad(4)$$

In a fairly large deflection problem, the membrane strains of the middle surface are given by[11]

$$\left.\begin{aligned}\varepsilon_{11m}&=(\alpha_1\alpha_2)^{-1}[\alpha_2U_{1,1}+\alpha_{1,2}U_2+\alpha_1\alpha_2R_1^{-1}W+1/2\alpha_1\alpha_2\phi_1^2+1/2\alpha_1\alpha_2\phi^2]\\\varepsilon_{22m}&=(\alpha_1\alpha_2)^{-1}[\alpha_1U_{2,2}+\alpha_{2,1}U_1+\alpha_1\alpha_2R_2^{-1}W+1/2\alpha_1\alpha_2\phi_2^2+1/2\alpha_1\alpha_2\phi^2]\\\varepsilon_{12m}&=1/2(\alpha_1\alpha_2)^{-1}[\alpha_2U_{2,1}+\alpha_1U_{1,2}-\alpha_{1,2}U_1-\alpha_{2,1}U_2+\alpha_1\alpha_2\phi_1\phi_2]\end{aligned}\right\},\quad(5)$$

where ε_{12m} is half the usual engineering shear strain. The bending distortions χ_{11}, χ_{22}, χ_{12} are[11]

$$\left.\begin{aligned}\chi_{11}&=(\alpha_1\alpha_2)^{-1}[\alpha_2\phi_{1,1}+\alpha_{1,2}\phi_2]\\\chi_{22}&=(\alpha_1\alpha_2)^{-1}[\alpha_1\phi_{2,2}+\alpha_{2,1}\phi_1]\\\chi_{12}&=1/2(\alpha_1\alpha_2)^{-1}[\alpha_2\phi_{2,1}+\alpha_1\phi_{1,2}-\alpha_{1,2}\phi_1\\&\quad-\alpha_{2,1}\phi_2+\alpha_1\alpha_2(R_2^{-1}-R_1^{-1})\phi]\end{aligned}\right\}.\quad(6)$$

Under the Kirchhoff-Love hypothesis and by neglecting the terms of order ζ/R_1 and ζ/R_2 relative to unity, the strains at the distance ζ from the middle surface, ε_{11}, ε_{22}, ε_{12} are

$$\left.\begin{aligned}\varepsilon_{11}&=\varepsilon_{11m}+\zeta\chi_{11}\\\varepsilon_{22}&=\varepsilon_{22m}+\zeta\chi_{22}\\\varepsilon_{12}&=\varepsilon_{12m}+\zeta\chi_{12}\end{aligned}\right\},\quad(7)$$

respectively.

Now, in order to introduce strain rate dependency and the Bauschinger effect in the plastic range, we shall use the equations by Perzyna[8] for the constitutive relation of each layer of the overlay model[9], as shown in Fig.2. This model corresponds to the

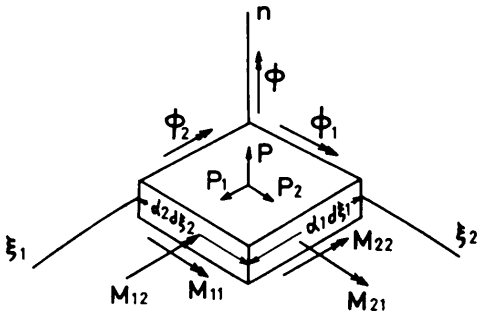

(a) Moments, rotations and loads

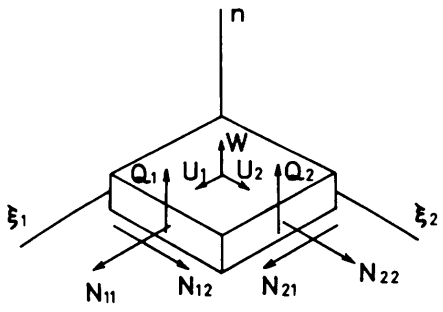

(b) Forces and displacements

Fig. 1 Coordinates and notations

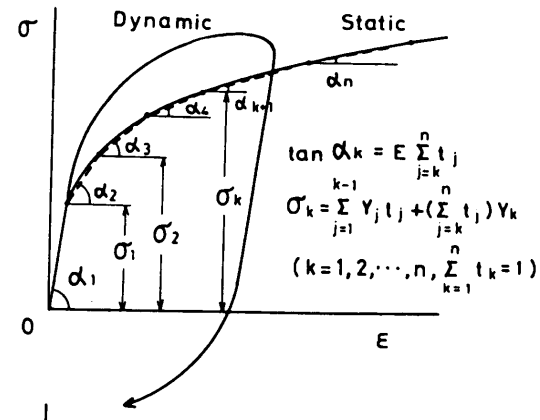

Fig. 2 Elasto/visco-plastic overlay model

kinematic hardening model whose yield surface does not expand. In the plane stress state assumed in the ordinary thin shell theory, the constitutive relations of each layer may be expressed as follows:

$$\begin{Bmatrix}\dot{\varepsilon}_{11}\\ \dot{\varepsilon}_{22}\\ \dot{\varepsilon}_{12}\end{Bmatrix}=\frac{1}{E}\begin{bmatrix}1 & -\nu & 0\\ -\nu & 1 & 0\\ 0 & 0 & 1+\nu\end{bmatrix}\begin{Bmatrix}\dot{\sigma}_{11k}\\ \dot{\sigma}_{22k}\\ \dot{\sigma}_{12k}\end{Bmatrix}+\begin{Bmatrix}\dot{\varepsilon}^{vp}_{11k}\\ \dot{\varepsilon}^{vp}_{22k}\\ \dot{\varepsilon}^{vp}_{12k}\end{Bmatrix}, \tag{8}$$

where E is Young's modulus, ν is Poisson's ratio and

$$\begin{Bmatrix}\dot{\varepsilon}^{vp}_{11k}\\ \dot{\varepsilon}^{vp}_{22k}\\ \dot{\varepsilon}^{vp}_{12k}\end{Bmatrix}=\gamma_k<\Psi(f_k)>\frac{1}{\bar{\sigma}_k}\begin{bmatrix}1 & -0.5 & 0\\ -0.5 & 1 & 0\\ 0 & 0 & 1.5\end{bmatrix}\begin{Bmatrix}\sigma_{11k}\\ \sigma_{22k}\\ \sigma_{12k}\end{Bmatrix} \tag{9}$$

$$f_k=(\bar{\sigma}_k-\sigma_{Yk})/\sigma_{Yk} \tag{10}$$

$$\bar{\sigma}_k=(\sigma^2_{11k}+\sigma^2_{22k}-\sigma_{11k}\sigma_{22k}+3\sigma^2_{12k})^{1/2}. \tag{11}$$

The dots in these equations denote the partial differentiation with respect to time, and the indices k in the material constant γ_k, the stress σ_k and the visco-plastic strain ε^{vp}_k mean the kth layer of the overlay model. The symbol $<\Psi(f_k)>$ is defined as follows:

$$\left.\begin{aligned}&<\Psi(f_k)>=0 \quad \text{when} \quad f_k\leqq 0\\ &<\Psi(f_k)>=\Psi(f_k) \quad \text{when} \quad f_k>0\end{aligned}\right\}, \tag{12}$$

and $f_k=0$ denotes the von Mises yield surface, while $\bar{\sigma}_k$ and σ_{Yk} are the equivalent stress and the yield stress in uniaxial reversal loading tests with very small strain rate, respectively.

Solving Eq.(8) for stresses, the stresses in each layer are

$$\begin{Bmatrix}\dot{\sigma}_{11k}\\ \dot{\sigma}_{22k}\\ \dot{\sigma}_{12k}\end{Bmatrix}=\frac{E}{1-\nu^2}\begin{bmatrix}1 & \nu & 0\\ \nu & 1 & 0\\ 0 & 0 & 1-\nu\end{bmatrix}\left(\begin{Bmatrix}\dot{\varepsilon}_{11}\\ \dot{\varepsilon}_{22}\\ \dot{\varepsilon}_{12}\end{Bmatrix}-\begin{Bmatrix}\dot{\varepsilon}^{vp}_{11k}\\ \dot{\varepsilon}^{vp}_{22k}\\ \dot{\varepsilon}^{vp}_{12k}\end{Bmatrix}\right). \tag{13}$$

Multiplying the stresses $\sigma_{11k}\sim\sigma_{12k}$ by the thickness t_k of the k th layer and summing up these values of each layer, the stresses at a generic point in the shell are

$$\{\sigma_{11},\ \sigma_{22},\ \sigma_{12}\}=\sum_{k=1}^{n}\{\sigma_{11k},\ \sigma_{22k},\ \sigma_{12k}\}t_k,\quad \sum_{k=1}^{n}t_k=1. \tag{14}$$

The resultant stresses and the resultant moments per unit length are as follows:

$$N_{ij}=\int_{-h/2}^{h/2}\sigma_{ij}d\zeta,\ M_{ij}=\int_{-h/2}^{h/2}\sigma_{ij}\zeta d\zeta \quad (i,j=1,2). \tag{15}$$

A complete set of field equations for 30 independent variables, N_{11}, N_{22}, N_{12}, M_{11}, M_{22}, M_{12}, U_1, U_2, W, ε_{11}, ε_{22}, ε_{12}, ε_{11m}, ε_{22m}, ε_{12m}, χ_{11}, χ_{22}, χ_{12}, ϕ_1, ϕ_2, ϕ, σ_{11}, σ_{22}, σ_{12}, σ_{11k}, σ_{22k}, σ_{12k}, ε^{vp}_{11k}, ε^{vp}_{22k}, ε^{vp}_{12k}, is now given by 30 equations, (3)$\sim$(7), (9) and (13)$\sim$(15).

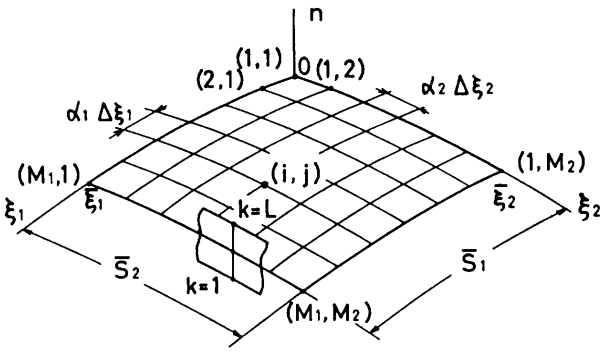

Fig. 3 Mesh points (i,j,k)

3. Numerical Method

If we solve the above 30 equations with suitable boundary conditions, we have solutions for the problem. However, it is too difficult to solve these equations analytically, so we shall use the finite difference method.

Let the shell be divided into (M_1-1) and (M_2-1) equal segments in the direction of ξ_1 and ξ_2, as shown in Fig. 3. Then the increments $\Delta\xi_1$, and $\Delta\xi_2$ in the nondimensional variables ξ_1 and ξ_2 are as follows:

$$\Delta\xi_1=\frac{\bar{s}_1}{\alpha_1(M_1-1)},\ \Delta\xi_2=\frac{\bar{s}_2}{\alpha_2(M_2-1)}, \tag{16}$$

where $\bar{s}_1,\bar{s}_2$ are the lengths of the shell in the directions of ξ_1, ξ_2, respectively.

In order to use Simpson's 1/3 rule for integration of Eq.(15), we divide the thickness h of the shell into $(L-1)$ equal layers, running from 1 at the inner surface to L at the outer surface. Then the positions of arbitrary points of the shell may be written as (i,j,k).

Denoting some quantities at the mesh point (i,j) by f_{ij} and employing three point difference formulas for the boundary and central difference formulas for other points, nine finite difference equations related to four boundary lines*, four boundary corner points** and the region except the boundary can be obtained for each derivative: $\partial f_{ij}/\partial\xi_1$, $\partial f_{ij}/\partial\xi_2$, $\partial^2 f_{ij}/\partial\xi_1^2$, $\partial^2 f_{ij}/\partial\xi_2^2$, $\partial^2 f_{ij}/\partial\xi_1\partial\xi_2$. For the second derivatives with respect to time in the inertia terms in Eq.(3), the next relation is employed:

$$\partial^2 f/\partial t^2=\frac{1}{(\Delta t)^2}(f_{t-\Delta t}-2f_t+f_{t+\Delta t}). \tag{17}$$

By the use of the above finite difference equations, the equations of motion (Eq.(3)) are transformed into the following equations at the point (i,j):

$$\left.\begin{aligned}U_1(t+\Delta t)=&-U_1(t-\Delta t)+2U_1(t)+\{\Delta t^2/(\alpha_1\alpha_2\rho_0 h)\}[a_1N_{11}(t)+a_2N_{11}(t)_{,1}+a_3N_{11}(t)_{,2}+a_4N_{22}(t)\\ &+a_5N_{22}(t)_{,2}+a_6N_{12}(t)+a_7N_{12}(t)_{,2}+a_8M_{11}(t)+a_9M_{11}(t)_{,1}+a_{10}M_{22}(t)+a_{11}M_{12}(t)+a_{12}M_{12}(t)_{,2}+a_{13}P_1(t)]\\ W(t+\Delta t)=&-W(t-\Delta t)+2W(t)+\{\Delta t^2/(\alpha_1\alpha_2\rho_0 h)\}[c_1N_{11}(t)+c_2N_{11}(t)_{,1}+c_3N_{22}(t)+c_4N_{22}(t)_{,2}\\ &+c_5N_{12}(t)+c_6N_{12}(t)_{,1}+c_7N_{12}(t)_{,2}+c_8M_{11}(t)_{,11}+c_9M_{22}(t)_{,22}+c_{10}M_{12}(t)_{,12}+c_{11}P(t)]\end{aligned}\right\}, \tag{18}$$

* $[\xi_1=0,\ \bar{\xi}_1,\ \xi_2=0,\ \bar{\xi}_2]$

** $[(\xi_1,\xi_2)=(0,0),(\bar{\xi}_1,0),(0,\bar{\xi}_2),(\bar{\xi}_1,\bar{\xi}_2)]$

and so on, where the coefficients $a_i(i, j)$ and $c_i(i, j)$ consist of the constants determined from the shell form and the rotations at time $T=t$. From Eq.(18), if each displacement at time $T=t-\Delta t$ and t, and each internal force at time $T=t$ are known at every spatial mesh point (i, j), the displacements at time $T=t+\Delta t$ can be calculated.

When each displacement at $T=t+\Delta t$ is obtained, the increments of displacements are evaluated from the next equations,

$$\delta U_1(i, j, t)=U_1(i, j, t+\Delta t)-U_1(i, j, t), \tag{19}$$

and so on.

The incremental strains $\delta\varepsilon_{ij}$ at any point (i,j,k) are as follows from Eqs.(4)～(7):

$$\left.\begin{aligned}
&\delta\varepsilon_{11}(i, j, k, t)=(\alpha_1\alpha_2)^{-1}[\alpha_2\delta U_1(i, j, t)_{,1}+\alpha_{1,2}\delta U_2(i, j, t)+\alpha_1\alpha_2 R_1^{-1}\delta W(i, j, t)]+\phi_1(i, j, t)\delta\phi_1(i, j, t)\\
&\quad+\frac{1}{2}\delta\phi_1^2(i, j, t)+\phi(i, j, t)\delta\phi(i, j, t)+\frac{1}{2}\delta\phi^2(i, j, t)+h\left(\frac{k-1}{L-1}-\frac{1}{2}\right)(\alpha_1\alpha_2)^{-1}[\alpha_2\delta\phi_1(i, j, t)_{,1}+\alpha_{1,2}\delta\phi_2(i, j, t)]\\
&\delta\varepsilon_{12}(i, j, k, t)=\frac{1}{2}(\alpha_1\alpha_2)^{-1}[-\alpha_{1,2}\delta U_1(i, j, t)+\alpha_1\delta U_1(i, j, t)_{,2}-\alpha_{2,1}\delta U_2(i, j, t)+\alpha_2\delta U_2(i, j, t)_{,1}]\\
&\quad+\frac{1}{2}\phi_1(i, j, t)\delta\phi_2(i, j, t)+\frac{1}{2}\delta\phi_1(i, j, t)\phi_2(i, j, t)+\frac{1}{2}\delta\phi_1(i, j, t)\delta\phi_2(i, j, t)\\
&\quad+h\left(\frac{k-1}{L-1}-\frac{1}{2}\right)\frac{1}{2}(\alpha_1\alpha_2)^{-1}[\alpha_2\delta\phi_2(i, j, t)_{,1}+\alpha_1\delta\phi_1(i, j, t)_{,2}-\alpha_{1,2}\delta\phi_1(i, j, t)-\alpha_{2,1}\delta\phi_2(i, j, t)\\
&\quad+\alpha_1\alpha_2(R_2^{-1}-R_1^{-1})\delta\phi(i, j, t)]
\end{aligned}\right\}, \tag{20}$$

and so on.

From the incremental strains $\delta\varepsilon_{ij}$ and the stresses σ_{ijk} in each layer of the overlay model, the incremental stresses of esch layer are obtained by using Eqs.(9) and (13). Adding these to the stresses of each layer at time $T=t$, we obtain the stresses σ_{ijk} in each layer at time $T=t+\Delta t$.

The stresses at any point in the shell at time $T=t+\Delta t$ are evaluated by summing the forces of each layer through Eq.(14), and each internal force at time $T=t+\Delta t$ is calculated from numerical integration of Eq.(15) by Simpson's 1/3 rule. Substituting these internal forces into Eq.(18), we obtain the displacements at the next time.

Now the initial displacements (incremental displacements) at time $T=\Delta t$ must be given for this calculation. In order to reduce the error in the initial approximation, we divide the first time increment into several equal parts: $\Delta t_0=\Delta t/n$ (e.g., $n=10$). The loading which is considered in this analysis may be either impulsive or of finite duration. A general case of impulsive loading is denoted by impulse $I(\xi_1, \xi_2)$ per unit area. Since all displacements are assumed to be zero in the beginning, initial incremental displacements may be given by

$$\left.\begin{aligned}
U_1&=\delta U_1=\frac{I_1(\xi_1, \xi_2)}{\rho_0 h}\Delta t_0=\dot{U}_1\Delta t_0\\
U_2&=\delta U_2=\frac{I_2(\xi_1, \xi_2)}{\rho_0 h}\Delta t_0=\dot{U}_2\Delta t_0\\
W&=\delta W=\frac{I(\xi_1, \xi_2)}{\rho_0 h}\Delta t_0=\dot{W}\Delta t_0
\end{aligned}\right\}. \tag{21}$$

If the shell is excited by applied surface loads, initial conditions become as follows:

$$\left.\begin{aligned}
U_1&=\delta U_1=\frac{P_1\Delta t_0^2}{2\rho_0 h}\\
U_2&=\delta U_2=\frac{P_2\Delta t_0^2}{2\rho_0 h}\\
W&=\delta W=\frac{P\Delta t_0^2}{2\rho_0 h}
\end{aligned}\right\}. \tag{22}$$

4. Numerical Example

As a numerical example, a 1100-O aluminum cylindrical shell under a semisinusoidal load with respect to time, as shown in Fig. 4, is analyzed. The

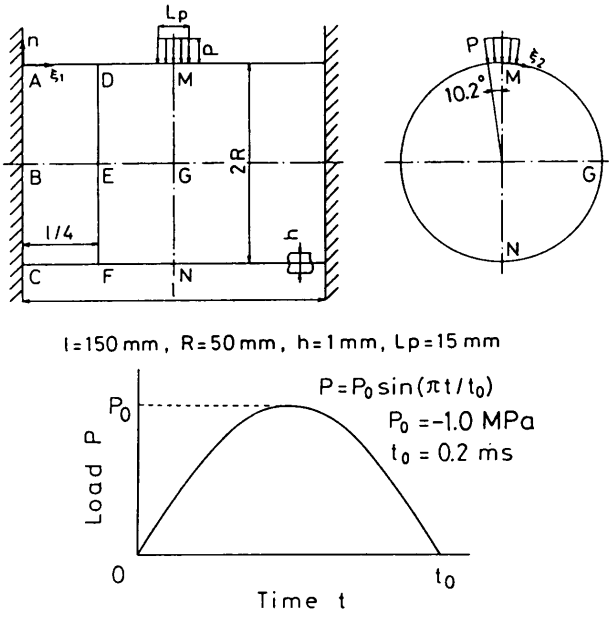

Fig. 4 Cylindrical shell and loading

load is locally distributed, and the ends of the shell are assumed to be fixed.

As for the coordinates, we shall take ξ_1 in the direction of axis (ξ) and ξ_2 in the direction of circumference (θ). The problem being symmetric with respect to two planes, it is sufficient to calculate only a quarter of the shell (ACNM), and the geometrical parameters for this portion are as follows:

$$\left.\begin{aligned} &A_1=A_2=R,\ \Delta\xi=l/2R(M_1-1)\\ &\Delta\theta=\pi/(M_2-1),\ R_1=\infty,\ R_2=R \end{aligned}\right\}. \tag{23}$$

The boundary conditions are,

$$\left.\begin{aligned} &\text{for the fixed edge AC:}\\ &\quad U_\xi=U_\theta=W=\partial W/\partial\xi=0;\\ &\text{for the symmetrical plane MN:}\\ &\quad U_\xi=\partial U_\theta/\partial\xi=\partial W/\partial\xi=0;\\ &\text{for the symmetrical plane AMNC:}\\ &\quad U_\theta=\partial U_\xi/\partial\theta=\partial W/\partial\theta=0 \end{aligned}\right\}. \tag{24}$$

The initial conditions may be given by

$$\left.\begin{aligned} &t=0: U_\xi=U_\theta=W=0\\ &t=\Delta t: U_\xi=\delta U_\xi=0,\ U_\theta=\delta U_\theta=0\\ &\qquad W=\delta W=\frac{P\Delta t^2}{2\rho_0 h}=\frac{P_0\Delta t^2\sin(\pi\Delta t/t_0)}{2\rho_0 h} \end{aligned}\right\}. \tag{25}$$

The model which consists of 6 layers[10] is employed in this example and the material constants of each layer of the model are decided as follows, from tension tests on Al 1100-O with various strain rates:

$$\left.\begin{aligned} &E=70.0\ \text{GPa},\ \nu=0.33,\ \rho_0=2.71\ \text{g/cm}^3\\ &\sigma_{Yk}=[\sigma_{Y1}\sim\sigma_{Y6}]=[15.7, 25.5, 38.8, 59.5, 99.3, 213]\ (\text{MPa})\\ &t_k=[t_1\sim t_6]=[0.778, 0.070, 0.046, 0.035, 0.030, 0.041]\\ &\gamma_k=[\gamma_1\sim\gamma_6]=[45.0, 39.7, 35.4, 30.3, 24.6, 19.1]\ (1/\text{s})\\ &\Psi(f_k)=\left(\frac{\bar\sigma_k-\sigma_{Yk}}{\sigma_{Yk}}\right)^{2.0} \end{aligned}\right\}. \tag{26}$$

From the obtained stress-strain curves, the constitutive relation of the single-layered model (isotropic hardening model) becomes

$$\left.\begin{aligned} &\begin{Bmatrix}\dot\varepsilon_\xi^{vp}\\ \dot\varepsilon_\theta^{vp}\\ \dot\varepsilon_{\xi\theta}^{vp}\end{Bmatrix}=\frac{2}{\sqrt{3}}\gamma_0<\Psi(f)>\frac{1}{\bar\sigma}\begin{bmatrix}1 & -0.5 & 0\\ -0.5 & 1 & 0\\ 0 & 0 & 1.5\end{bmatrix}\begin{Bmatrix}\sigma_{\xi k}\\ \sigma_{\theta k}\\ \sigma_{\xi\theta k}\end{Bmatrix},\\ &\Psi(f)=\{(\bar\sigma-\sigma^*)/\sigma^*\}^{2.0},\ \gamma_0=61\ 1/\text{s}\\ &\sigma^*=112(0.002\,98+\bar\varepsilon^{vp})^{0.245}\ \text{MPa} \end{aligned}\right\}, \tag{27}$$

where $\bar\varepsilon^{vp}$ is an equivalent visco-plastic strain. The stress-strain curves of the material given by Eqs. (26) and (27) under uniaxial tension and under uniaxial cyclic loading are shown in Figs. 5 and 6. It is found from Fig. 6 that approximations to the Bauschinger effect and the strain rate dependency in the plastic range can be obtained by using the elasto/visco-plastic overlay model.

Mesh point numbers M_1, M_2 and the division number L through thickness are $M_1=26$, $M_2=45$ and $L=17$, respectively. The increment of time Δt is set as 5.0×10^{-4} ms.

Now we shall discuss the results of calculation. The calculations are carried out to 0.8 ms for two material models, the isotropic hardening model and the overlay model. Some of the essential features of the solutions are shown in Figs. 7~12. In these figures, the results from the overlay model are indicated by solid lines and chain lines, and the results from the isotropic hardening models are indicated by broken lines.

Maximum values (absolute values) of strain and strain rate appear in the circumferential components

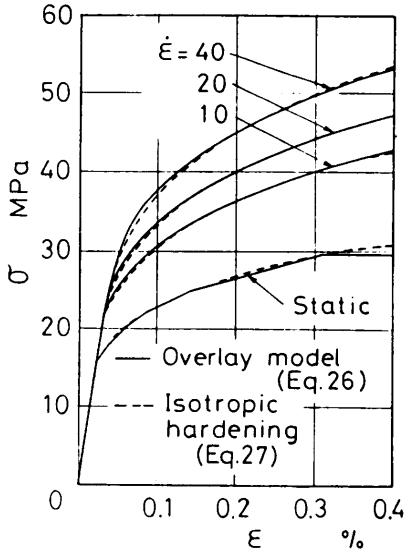

Fig. 5 Stress-strain relationships ($\dot\varepsilon$: constant)

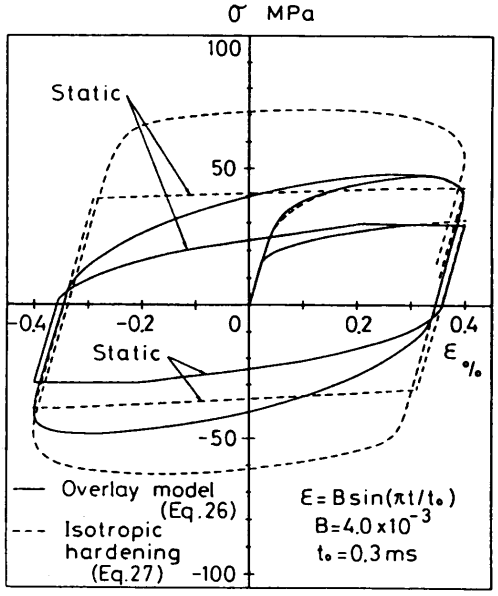

Fig. 6 Stresses under cyclic strain

at point M on the outer surface, and these values are 0.41% and 42 1/s, respectively.

Figure 7 shows the variations with time of W at points M, G and N, U_θ at point G and U_ξ at point D. U_ξ and U_θ are very small compared with W. In the middle cross section MGN, the shell begins to deform in the order of points M, G, N with the lapse of time, and large displacement occurs at point M, where the load is distributed. The difference between the solutions from the overlay model and the isotropic hardening model becomes marked at point M after $t=0.2$ ms, but becomes small at points G and N. It is found from the variations of W at point M and U_ξ at point D that the difference between the results from both models becomes nearly constant after $t=0.4$ ms, and that the isotropic hardening model estimates the return at about $t=0.4$ ms to be small.

Figures 8(a) and (b) give the variations of deformations in meridional section $\theta=0°$ and in the middle cross section $\xi=1.5$ with time, respectively. The shell deforms greatly inward near point M at $t=$ 0.18 ms, and the difference between the solutions from both models appears with the lapse of time. This difference is large near point M, but very small in the GN part.

Figure 9 represents the variations of N_ξ at points A, B and M, and N_θ at points A and M with time. N_ξ and N_θ at point M initially show large compression, and after $t=0.2$ ms a difference between the results

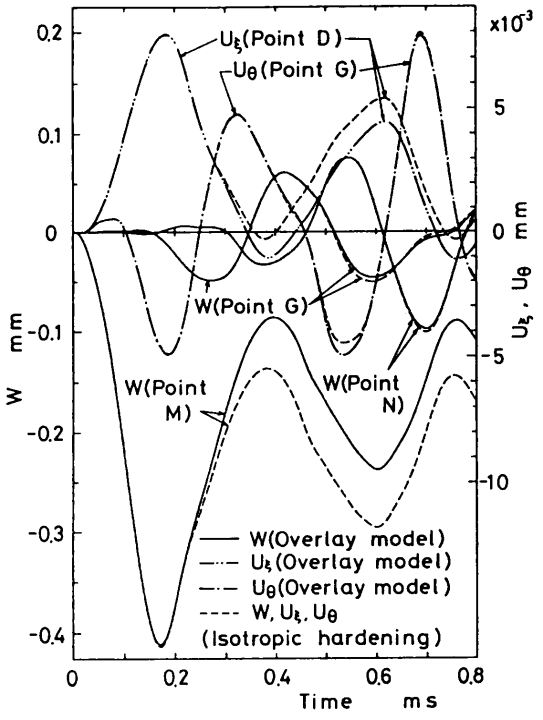

Fig. 7 Variations of displacements at points M, G, N, D with time

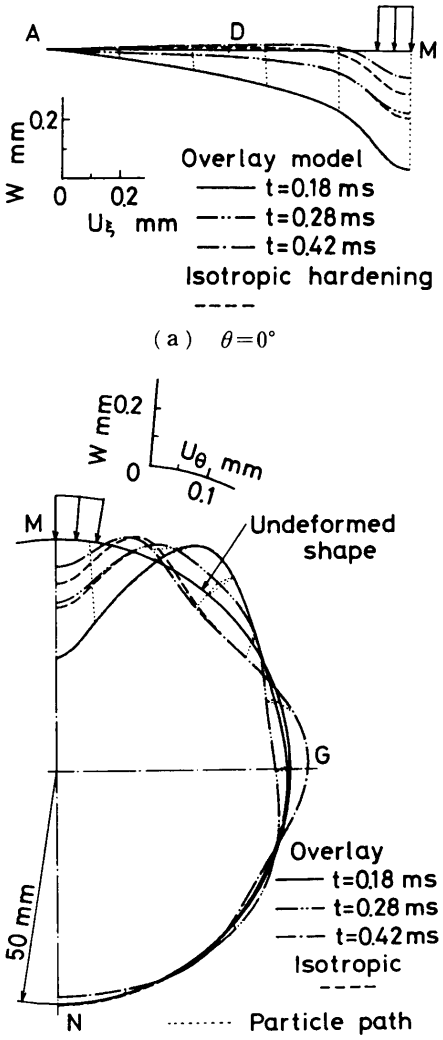

(a) $\theta=0°$

(b) $\xi=1.5$

Fig. 8 Variations of deformations with time

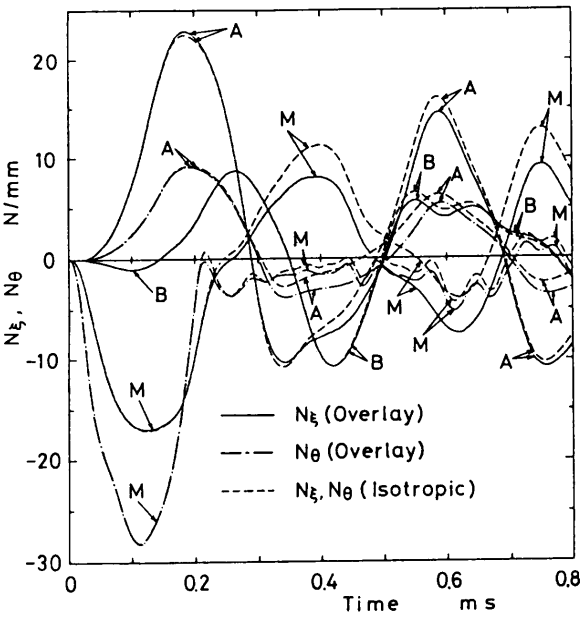

Fig. 9 Variations of N_ξ, N_θ with time

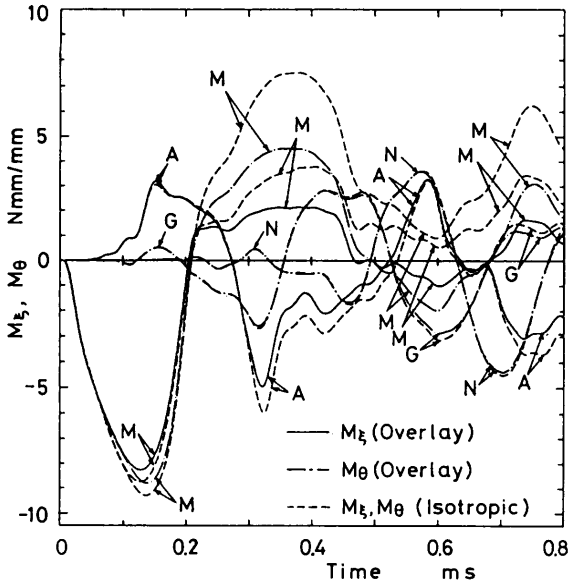

Fig. 10 Variations of M_ξ, M_θ with time

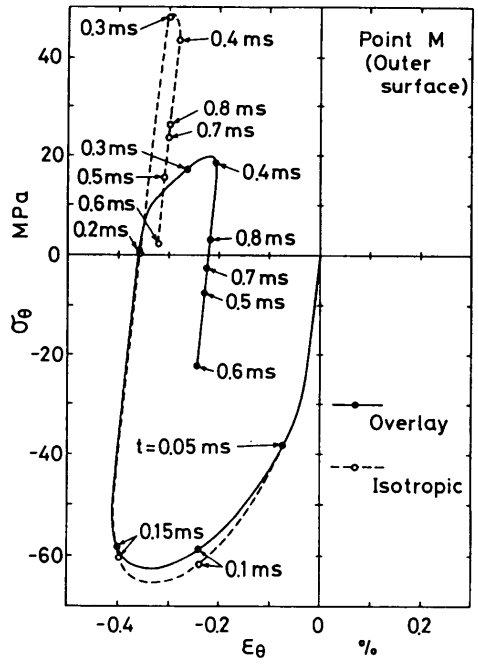

Fig. 11 $\sigma_\theta - \varepsilon_\theta$ relationships on outer surface at point M

from both models appears. On the other hand, these components at point A indicate large tension at first, and the difference appears after about $t=0.3$ ms. It is seen from the variation of N_ξ at point M that in the case of the isotropic hardening model, mean value of vibration is larger than that in the case of the overlay model.

Figure 10 shows the variations of M_ξ at points A and M, and M_θ at points M, G and N. The large difference between the results from both models is observed at points A and M, and this difference generally appears after $t=0.2$ ms at point M and about $t=0.3$ ms at point A, as well as in the case of the resultant stresses. Some difference appears about $t=0.1$ ms at point M, though reyielding does not occur. It seems that this is due to the difference between the stress-strain curves of the two models shown in Fig. 5.

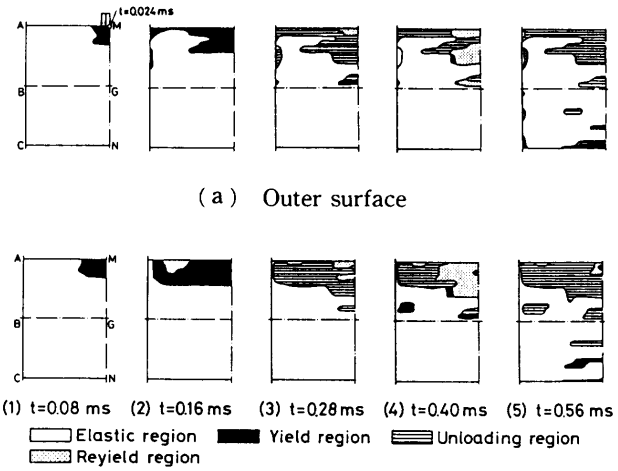

Fig. 12 Progression of yield with time (by overlay model)

$\sigma_\theta - \varepsilon_\theta$ relationships on the outer surface at point M are plotted in Fig. 11. The large difference between the results from the overlay model and those from the isotropic hardening model appears after reyielding. This fact corresponds to the difference between the solutions for displacements and internal forces from both models at point M after $t=0.2$ ms, as shown in Figs. 7~10. At about $t=0.1$ ms, some difference between the solid and broken lines is found. It seems that this is due to the difference between the stress-strain curves of the two models as well as the bending moments in Fig. 10.

Figures 12(a) and (b) illustrate the aspect of progression of yielding on the inner and outer surfaces of the shell by the overlay model. In these figures, the unloading region means the portion where the equivalent stress becomes smaller than the yield stress after yielding. The aspect of progression of yielding by the isotropic hardening model, not illustrated here, is almost the same as this figure. At first, yielding occurs on the outer surface at point M and then the yield region expands in the meridional direction. At about $t=0.28$ ms, yielding occurs near point G, and later it appears on the inner and outer surfaces at point N. Unloading and reyielding appear alternately with time in the yield region of the shell.

The numerical calculation for the present example requires about 42 minutes in the case of the overlay model and about 10 minutes in the case of the

isotropic hardening model on FACOM VP-200.

5. Conclusions

In this paper, we have described the numerical analysis on the elasto/visco-plastic dynamic response of general thin shells to arbitrary blast loads by the use of the elasto/visco-plastic overlay model, which is able to express the Bauschinger effect and the strain rate dependency. The equations of motion and the strain-displacement relations have been derived from Sanders, nonlinear theory for thin shells. The numerical method selected for this problem is a method using finite difference in both space and time.

As a numerical example, an aluminum cylindrical shell under a semisinusoidal external load with respect to time was analyzed for two material models, the isotropic hardening model and the overlay model. It was found from the calculated results that in the case of reversal stress, a difference between the results from the two material models is evident, and the isotropic model estimates the variation of displacements to be small and the variation of internal forces to be large immediately after reyielding.

References

(1) Nagarajan, S. and Popov, E. P., Non-Linear Dynamic Analysis of Axisymmetric Shells, Int. J. Numer. Method in Eng., Vol. 9, No. 3 (1975), p. 535.

(2) Takezono, S. and Tao. K., Elasto/Visco-Plastic Dynamic Response of Shells of Revolution, Trans. 4 th Int. Conf. on Struct. Mech. in Reactor Tech., M 7/7(1977), p. 1.

(3) Atkatsh, R. S., Bieniek, M. P. and Sandler, I. S., Theory of Viscoplastic Shells for Dynamic Response, Trans. ASME. Ser. E, Vol. 50, No. 1 (1983), p. 131.

(4) Wojewódzki, W. and Bukowski, R., Influence of the Yield Function Nonlinearity and Temperature in Dynamic Buckling of Viscoplastic Cylindrical Shells, Trans. ASME, Ser. E, Vol. 51, No. 1 (1984), p. 114.

(5) Tao, K., Takezono, S. and Uchibori, H., Elasto/Visco-Plastic Dynamic Response of Moderately Thick Shells of Revolution under Consideration of Rotatory Inertia, Proc. Int. Conf. on Comput. Eng. Sci., 2, 41, ii (1988), p. 1.

(6) Tao, K., Takezono, S., Taguchi, T. and Hotada, K., Elasto/Visco-Plastic Dynamic Response of Axisymmetrical Shells Under Mechanical and/or Thermal Loading, JSME Int. J., Vol. 32, No. 3 (1989), p. 341.

(7) Takezono, S. and Tao, K., Elasto/Visco-Plastic Dynamic Response of General Thin Shells to Blast Loads, Bull. JSME, Vol. 25, No. 203 (1982), p. 728.

(8) Perzyna, P., Fundamental Problems in Viscoplasticity, Adv. Appl. Mech., Vol. 9 (1966), p. 243, Academic Press.

(9) Besseling, J. F., A Theory of Elastic, Plastic, and Creep Deformations of an Initially Isotropic Material Showing Anisotropic Strain-Hardening, Creep Recovery, and Secondary Creep, Trans. ASME, Ser. E, Vol. 25, No. 4 (1958), p. 529.

(10) Takezono, S., Tao, K. and Kanezaki, K., Elasto/Visco-Plastic Dynamic Response of Axisymmetrical Shells by Overlay Model, Trans. ASME, Ser. J, Vol. 102, No. 3 (1980), p. 257.

(11) Sanders, J. L., Nonlinear Theories for Thin Shells, Q. Appl. Math., Vol. 21, No. 1 (1963), p. 21.